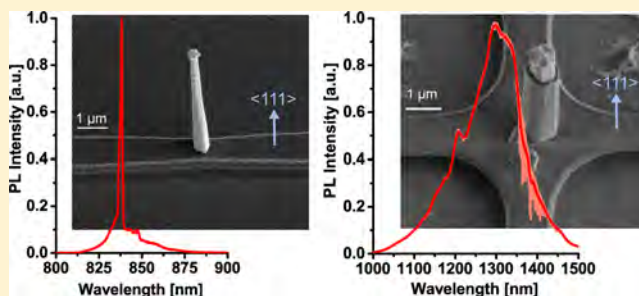


III–V Compound Semiconductor Nanopillars Monolithically Integrated to Silicon Photonics

Gilliard N. Malheiros-Silveira,^{1b} Fanglu Lu, Indrasen Bhattacharya, Thai-Truong D. Tran, Hao Sun, and Connie J. Chang-Hasnain^{*1b}

Department of Electrical Engineering and Computer Sciences, University of California, Berkeley, California 94720, United States

ABSTRACT: We propose a platform based on III–V compound semiconductor nanopillars monolithically integrated with silicon photonics. Nanopillars were grown in a process free of metal catalysts onto silicon at low temperature, and a bottom-up process was applied to define the photonic integrated circuit. Stimulated and spontaneous emissions from the nanopillars are direct coupled to silicon waveguides.



KEYWORDS: optical interconnects, silicon photonics, monolithic integration, quantum-well devices, optical links, nanopillar

Complementary metal-oxide-semiconductor (CMOS) process promoted the adoption of silicon as the preeminent platform by the microelectronics industry. The legacy of this technology is responsible for leveraging the implementation of active devices on silicon photonics.^{1,2} However, novel compact optical devices and very-low-energy optoelectronic devices are required for reducing the cost per bit while maximizing the processing ability of future silicon based electronic chips. In this context, optical interconnects are promising to play a substantial role in improving density, energy, and timing.³ The use of silicon as a standard platform brought many benefits both for microelectronics and photonics primarily because it makes it easier to scale up and integrate devices. However, as an optical material, silicon has an indirect band gap, which poses a tremendous limitation for efficient optoelectronic devices. To overcome this limitation, different strategies to integrate direct bandgap III–V compound materials onto a silicon platform have been proposed, which can be generally organized in the following categories: heteroepitaxial growth,^{4–14} wafer bonding,^{15,16} and flip-chip integration.¹⁷

Our approach to implement heterogeneous integration of III–V compound semiconductors onto silicon photonics is based on growth of nanopillars/nanoneedles/nanowires composed by active materials directly grown onto silicon substrate.^{5–8,10–14} Such approach substantially alleviates the effects of lattice mismatching between III–V compounds and silicon substrates, allowing the growth of high quality materials required for implementing efficient optoelectronic devices.^{18–21} In this letter, we propose and experimentally demonstrate a monolithic integration of III–V compound semiconductors in nano- and microscale geometries to silicon waveguide geometries, as well as the optical coupling of spontaneous^{10,11} and stimulated emission.¹⁰ A schematic of the proposed platform is

shown in Figure 1. Such platform can be obtained by two different approaches: top down (where nanopillars are grown in

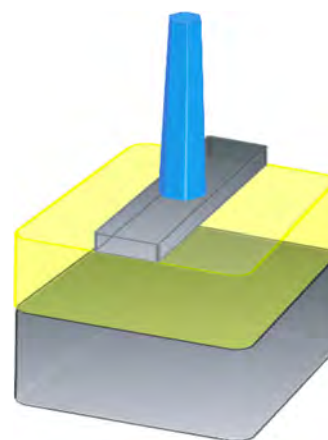


Figure 1. Scheme of III–V compound semiconductor nanopillar monolithically integrated to silicon waveguide.

specific positions on top of a silicon photonic circuit) or bottom up (where photonic circuit is defined after nanopillars growth). We present the latter approach where an optical source is monolithically integrated to silicon photonics platform. The results pave a new way for the realization of novel optical and optoelectronic devices which can fulfill the requirements of having ultracompact sources of light directly integrated to silicon photonics. The proposal and results show the complete compatibility with the CMOS platform as the

Received: December 25, 2016

Published: April 11, 2017

process is free of metal catalysts, it is performed at low temperatures, and it is cost-effective as it uses standard technologies like metal–organic chemical vapor deposition (MOCVD) to monolithically grow III–V onto silicon platform.

RESULTS AND DISCUSSION

Two different samples were grown in order to assess the aforementioned proposal. In the sample-1, InP nanopillars were grown onto a silicon substrate for short wavelength emission experiments. For the sample-2, InGaAs/InP quantum wells (QWs) on nanopillars were grown on a silicon-on-insulator (SOI) wafer in order to demonstrate silicon-transparent wavelength emission. Details about the preparation of samples and growth can be found in the [Methods](#).

The proposed process is shown in [Figure 2](#). After growing nanopillars ([Figure 2a](#)), sample is covered by 200 nm of SiO₂

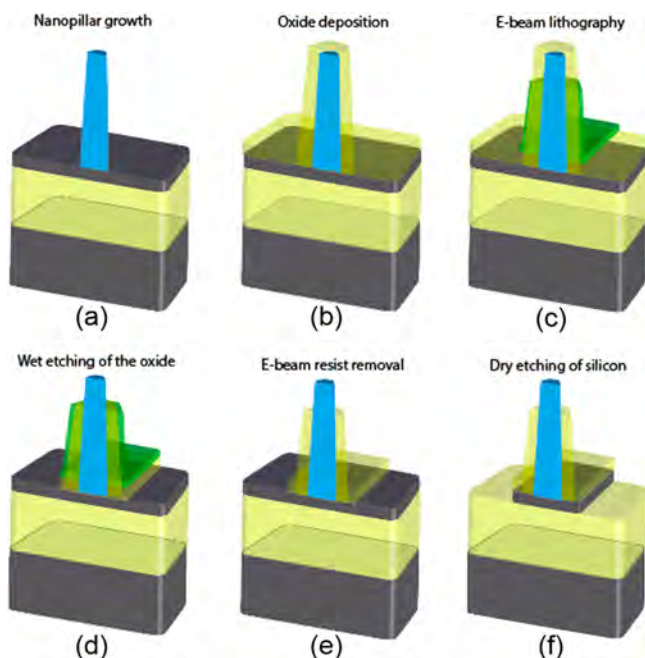


Figure 2. (a) Nanopillar grown by MOCVD. (b) Oxide deposition by PECVD. (c) Waveguide layout transferred by e-beam lithography using PMMA resist. (d) Transferring the waveguide pattern to SiO₂ layer by wet etching. (e) E-beam resist removal. (f) Dry etching of the silicon region by SF₆ and O₂ plasma.

layer, deposited by plasma-enhanced chemical-vapor deposition (PECVD) at 250 °C ([Figure 2b](#)) in order to produce a mask to define silicon waveguides. E-beam resist (PMMA) is spun with 4000 rpm for 60 s. After exposing and developing the e-beam resist ([Figure 2c](#)) the waveguide layouts are transferred to the SiO₂ layer by wet etching with buffered oxide etch (BOE) 10:1 for 3 min ([Figure 2d](#)). The higher portions of SiO₂ covering the nanopillars are also exposed to the wet etching due to the thickness and viscosity of the e-beam resist used to write the e-beam mask. Subsequently, both regions, Si(111) defined by the mask and the top portion of the nanopillars are exposed. E-beam resist is then removed by acetone, methanol and water ([Figure 2e](#)) and finally, a gas mixture of SF₆ (60 sccm) and O₂ (6 sccm) flows into a reactive ion etching (RIE) system in order to define the waveguide geometries in the silicon layer ([Figure 2f](#)). Since InP has a high selectivity against this plasma

mixture compared to silicon, the uncovered top regions of the nanopillars do not experience major etching related damages.

Time-Resolved Photoluminescence (TRPL) measurements were performed on the sample-1 in order to evaluate if the aforementioned process compromised the material quality of the nanopillars. [Figure 3](#) shows results from TRPL measure-

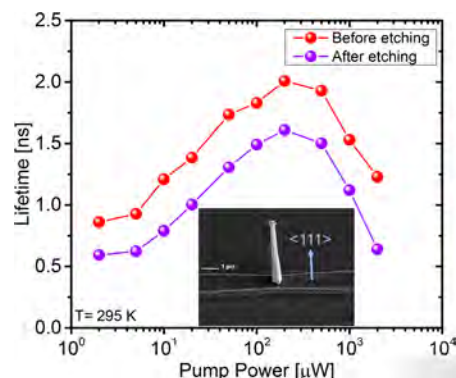


Figure 3. InP carrier lifetime comparison: before and after the process applied to realize the waveguides on the sample-1.

ments in one of the structures, where the lifetime from the InP nanopillar is compared before and after the waveguides fabrication process. In general, a small change was seen within the reasonable range of optical pump power levels. The inset in [Figure 3](#) shows a SEM image (30° of tilted view) of a fabricated device (after removing the SiO₂ mask) with an up-right InP nanopillar positioned on top of a Si ridge waveguide geometry. The InP nanopillar has, at its bottom region, a diameter of 528 nm and a length of 6.45 μm and is positioned at the center of a silicon waveguide with a ridge thickness of 410 nm (measured by 3-D laser confocal microscope).

Microphotoluminescence (μ -PL) measurements performed on nanopillars on silicon waveguides are shown in [Figure 4a](#) (in blue): the emission is centered at $\lambda = 825$ nm at low temperature (4 K), indicating the pillar material is single crystalline and in Wurtzite phase. The inset shows a top-view SEM image from that structure. As the optical pumping power is increased, the nanopillar emission reaches threshold and lasing. The red curve in [Figure 4a](#) shows the narrowing of optical spectrum. The laser peak dominates the emission above the threshold, achieving about 7.88 dB of background suppression ratio. In [Figure 4b](#), the L–L curve from that nanopillar measured at 4 K has an abrupt “S-shape”, with laser threshold at 223 μ J/cm². Finally, camera images of a single InP nanopillar emission below threshold show just a spot of light from spontaneous emission ([Figure 4c](#)), and above threshold (upon lasing) strong speckle patterns can be noticed ([Figure 4d](#)). The speckle pattern results from high degree of coherent emission, a classic signature of laser oscillation.

Nanopillars grow along the $\langle 111 \rangle$ directions. While most pillars are grown surface-normal to the (111) Si-substrate, many others grow along a degenerate direction and form an angle of 54.7 degrees to the surface-normal direction. [Figure 5](#) shows results for two nanopillars on waveguide structures fabricated using sample-2: one pillar has vertical orientation while the other one is slanted. [Figure 5a](#) shows SEM image (30° tilted view) of an InGaAs/InP 5-QWs upright nanopillar on top of the center of two crossing silicon waveguides. The structure with those crossing waveguides has four output ports

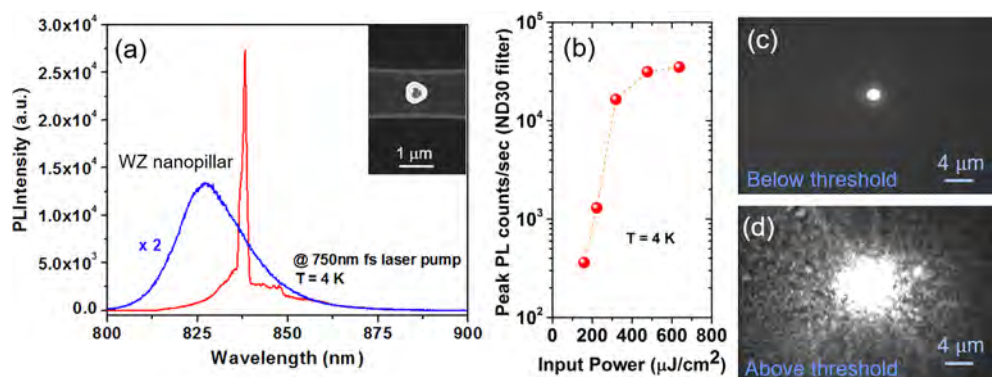


Figure 4. Optically pumped laser at low temperature after the process of fabrication as a proof that such process is robust, and does not compromise the material quality. (a) Spectra of the InP nanopillar laser below (blue, magnified 2 \times) and above (red) laser threshold measured at 4 K. Inset shows an SEM image from the top view of that structure. (b) L–L curve of the nanopillar laser. Camera images from the near field of the nanopillar laser below (c) and above the laser threshold (d).

(S_1 , S_2 , S_3 , and S_4), and a SiO_2 cladding layer partially covering the nanopillar can be noticed (as depicted in the schematic of the Figure 2f). This nanopillar has, at its bottom region, a diameter of about $0.9 \mu\text{m}$, and height of $\sim 4.3 \mu\text{m}$, and has a hexagonal pyramidal frustum shape. Those silicon waveguides have width of $\sim 1 \mu\text{m}$, and height of $\sim 0.9 \mu\text{m}$, and are positioned on top of a buried oxide (BOX) layer of $2.2 \mu\text{m}$ of thickness. The optical power emitted from this nanopillar, after filtering the spectrum around the optical pump ($\lambda_p = 750 \text{ nm}$), is shown in top view in Figure 5b. Optical coupling through all four ports is observed.

Crossing waveguides were also designed below slanted pillars in order to create an asymmetry in the structure and highlight another advantaged of this approach. An SEM image from the top view of this structure is shown in Figure 5c. The light emitted from that nanopillar is shown in Figure 5d. Bright emission from the nanopillar can be seen and, some portion of it can be seen coming from the two crossing waveguides all the way to the four output ports: S_1 , S_2 , S_3 , and S_4 . It is interesting to notice that the nanopillar does not need to be upright in order to couple light through silicon waveguide. Furthermore, nanopillars in both configurations are working like a dielectric resonator nanoantenna,²² and composed of active materials, integrated to a dielectric waveguide. μ -PL intensities from both structures are shown in Figure 5e with spontaneous emission centered at $\lambda_0 = 1.260 \mu\text{m}$ (for the slanted nanopillar) and $\lambda_0 = 1.300 \mu\text{m}$ (for the upright one) with peaks highlighting the presence of optical modes.

Figure 6 presents results from finite-difference time-domain (FDTD) simulations where the dependence of quality factor and coupling efficiency of the proposed platform versus the SOI device layer thickness, t_i is shown. The nanopillar dimensions from the SEM image shown in Figure 5a were taken as reference to perform the numerical simulations. As the slab thickness increases the quality factor decreases, the reason is because the mode in the nanopillar experiences less feedback from the reflections in very bottom face of the waveguide, making it easier to leak through the waveguide. From those simulations, the coupling efficiency through the waveguide reaches values as high as 30%, and most of the remaining stored power is radiated into free space. Figure 6b depicts the E_z -field from the resonating mode, quasi- TM_{41} , estimated from simulations. Figure 6c shows a colormap of the E-field magnitude stored in the nanopillar being coupled to the waveguide. Optimization in the waveguide portion around the

nanopillar, as well as the nanopillar geometry can increase the power coupled to waveguides like ridge and wire ones. Also, by optimizing the nanopillar geometry and dimensions (see Supporting Information in ref 6 and refs 13 and 14) it could be possible promote lasing activity and allow for low threshold laser emission, and increase the optical power leaked from the very bottom region of the nanopillar (which may increase the coupling efficiency). As an example of optimized nanopillar geometry, if we assume a hexagonal prism shape with a diameter of $0.88 \mu\text{m}$ and a height of $0.84 \mu\text{m}$ on top of the fabricated waveguide, the same mode, quasi- TM_{41} , would resonate at about $\lambda = 1.3 \mu\text{m}$ and would reach 60% of coupling efficiency, and quality factor of 52.

For the simulations shown in Figure 6, the nanopillar was modeled as an optical cavity acting as a source of light directly integrated to the silicon photonics platform. Furthermore, nanopillars with more tapered geometries, like that one shown at the inset from Figure 3, even if composed only by InP can be used as ultracompact passive optical couplers, for long-wavelength operation, in photonic integrated circuits.

CONCLUSION

We have experimentally demonstrated an ultracompact platform for coupling spontaneous and stimulated emission to silicon waveguides by directly growing III–V compound semiconductor nanopillars onto the silicon photonics platform. The fabricated sources of light assume footprints below $1 \mu\text{m}^2$ for long-wavelength emission in a CMOS compatible process, which represents a step toward of monolithic integration of efficient sources of light to silicon. In fact, an active nanopillar can be seen as an unprecedented all-dielectric resonator nanoantenna, which shines light to a perspective of collecting and converting light to be coupled in and out of waveguides. The experiments show that energy can be harvested by a nanopillar and coupled to waveguides in a structure with small footprint, which is another contribution in terms of device miniaturization. An optical coupler and a power splitter with four outputs (the number of output ports is not necessarily limited to four), can be monolithically integrated on a footprint as small as $\sim 4 \mu\text{m}^2$. Moreover, when such nanopillars/nanoneedles geometries are optically excited in their transparent window, they can behave like an optical passive coupler. In this perspective, they are still ultracompact compared to

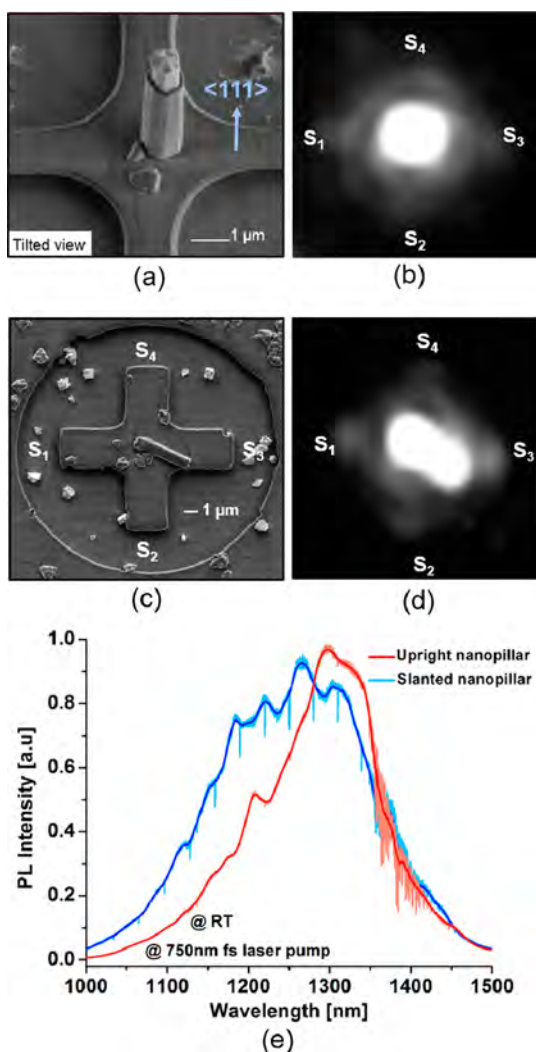


Figure 5. (a) SEM image from 30° tilted view of an upright nanopillar on top (and at center) of two crossing silicon waveguides. (b) Near field from μ -PL showing spontaneous emission from the nanopillar been coupled to the four waveguide outputs: S₁, S₂, S₃, and S₄. (c) SEM from the top view of a slanted pillar on top (and at center) of two crossing silicon waveguides. (d) Near field from μ -PL showing spontaneous emission from the nanopillar been coupled to the four waveguide outputs: S₁, S₂, S₃, and S₄. (e) μ -PL intensities of the device emitting light at the silicon transparent spectrum under excitation with 20 μ W of total power, which is spread over the beam spot.

grating couplers, and can be positioned at any location along an integrated optical circuit in contrast to inverse tapers.

METHODS

III–V Compound Semiconductor Growth. Nanopillars are grown in core–shell mode in a MOCVD reactor (Emcore D75) with InP acting as a growth template. For the sample-2, the InP core was designed to have a radius of 400 nm while the InP cladding was designed with a thickness of 75 nm. The InGaAs QWs were designed to have 5 nm of thickness, spaced by 7 nm of InP layers. All the heteroepitaxial growth was free of metal catalysts and occurred at 455 °C. Length and diameter scale almost linearly with growth time. Trimethylindium (TMIn), triethylgallium (TeGa), tertiarybutylarsine (TBAs), and tertiarybutylphosphine (TBP) were used as indium,

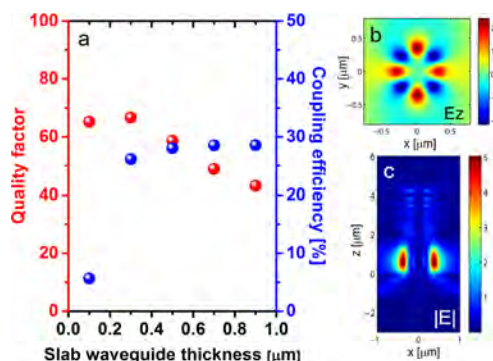


Figure 6. (a) Simulations showing the trade-off between the waveguide thickness versus quality factor and coupling efficiency. (b) Nanopillar cross-section outlining the resonating mode, TM₄₁ at $\lambda = 1.3 \mu\text{m}$. (c) Color map of the E-field magnitude distribution from the nanopillar to the waveguide assuming 0.9 μm of thickness.

gallium, arsenic, and phosphorus precursors, respectively. More details about the growth can be found in ref 7.

Optical Spectroscopy. The 120 fs pump pulses from a mode-locked Ti:sapphire laser (Coherent Mira, Ipump1/4 750 nm, repetition rate 76 MHz) were delivered to the samples by a 100 \times , 0.7 numerical aperture (NA) objective (Mitutoyo NIR HR). Nanopillar emission was collected by the same objective and relayed to a spectrometer and LN₂-cooled silicon charge-coupled device (Princeton Instruments SP2750 and Spec-10). Filters were used to prevent pump light from reaching any detectors and cameras. To achieve nanopillar laser oscillation at sample-1, the temperature was held at 4 K by a continuous-flow liquid-helium cryostat (Oxford Instruments Hi-Res II).

Numerical Simulations. Cavity simulations are performed using commercial FDTD simulation software (Lumerical) in order to evaluate general aspects of the optical feedback mechanism in nanopillars, as well as how efficiently light emitted from there can be coupled to silicon waveguides. The resonant mode is excited by positioning and aligning a single dipole source at one of the peaks of the mode. The source is pulsed and the time decay of the fields in the simulated structure is numerically calculated. Fourier analysis of the time decay reveals the frequency properties of the cavity and thus its resonances. Perfectly matched layers were introduced at the all boundaries. The calculation domain size is 7.00 \times 7.00 \times 13.00 μm^3 and the spatial resolution is 5 nm. A mode resonating at 1.30 μm (around the emission peak collected from PL in Figure 5e) is identified during the simulations and figures of merit like quality factor and coupling efficiency are numerically calculated when the thickness of a slab waveguide varies.

AUTHOR INFORMATION

Corresponding Author

*E-mail: cch@eecs.berkeley.edu.

ORCID

Gilliard N. Malheiros-Silveira: 0000-0002-5176-3812

Connie J. Chang-Hasnain: 0000-0002-5341-6267

Notes

The authors declare no competing financial interest.

ACKNOWLEDGMENTS

This work was supported by the National Science Foundation (NSF) Awards ECCS-0939514, 1335609, by the São Paulo Research Foundation (FAPESP) under grant 2013/03947-9,

and by the Singapore National Research Foundation Singapore–Berkeley Research Initiative for Sustainable Energy (SinBeRISE) Program NRF-CRP14-2014-03.

REFERENCES

- (1) Lipson, M. Guiding, Modulating, and Emitting Light on Silicon—Challenges and Opportunities. *J. Lightwave Technol.* **2005**, *23*, 4222–4238.
- (2) Bogaerts, W.; Baets, R.; Dumon, P.; Wiaux, V.; Beckx, S.; Taillaert, D.; Luyssaert, B.; Van Campenhout, J.; Bienstman, P.; Van Thourhout, D. Nanophotonic Waveguides in Silicon-on-Insulator Fabricated with CMOS Technology. *J. Lightwave Technol.* **2005**, *23*, 401–412.
- (3) Miller, D. Device Requirements for Optical Interconnects to Silicon Chips. *Proc. IEEE* **2009**, *97*, 1166–1185.
- (4) Razeghi, M.; Blondeau, R.; Defour, M.; Omnes, F.; Maurel, P.; Brillouet, F. First Room-Temperature CW Operation of a GaInAsP/InP Light-Emitting Diode on a Silicon Substrate. *Appl. Phys. Lett.* **1988**, *53*, 854.
- (5) Mårtensson, T.; Svensson, C. P. T.; Wacaser, B. A.; Larsson, M. W.; Seifert, W.; Deppert, K.; Gustafsson, A.; Wallenberg, L. R.; Samuelson, L. Epitaxial III–V Nanowires on Silicon. *Nano Lett.* **2004**, *4*, 1987–1990.
- (6) Chen, R.; Tran, T.-T. D.; Ng, K. W.; Ko, W. S.; Chuang, L. C.; Sedgwick, F. G.; Chang-Hasnain, C. Nanolasers Grown on Silicon. *Nat. Photonics* **2011**, *5*, 170–175.
- (7) Ren, F.; Tran, T.; Ng, K.; Li, K.; Sun, H.; Chang-Hasnain, C. J. High-Quality InP Nanoneedles Grown on Silicon. *Appl. Phys. Lett.* **2013**, *102*, 012115.
- (8) Lu, F.; Tran, T.-T. D.; Ng, K. W.; Gong, Z.; Chang-Hasnain, C. J. Long-Wavelength InGaAs/InP Quantum-Well-on-Nanopillar Laser Grown on Silicon. In *Compound Semiconductor Week 2015*; Santa Barbara, CA, 2015; p Tu4O5.3.
- (9) Wang, Z.; Tian, B.; Pantouvaki, M.; Guo, W.; Absil, P.; Van Campenhout, J.; Merckling, C.; Van Thourhout, D. Room-Temperature InP Distributed Feedback Laser Array Directly Grown on Silicon. *Nat. Photonics* **2015**, *9*, 837–842.
- (10) Malheiros-Silveira, G. N.; Lu, F.; Bhattacharya, I.; Tran, T.-T. D.; Sun, H.; Chang-Hasnain, C. J. *Integration of III-V Nanopillar Resonator to In-Plane Silicon Waveguides*; OSA: San Diego, CA, 2016; p STh1L.5.
- (11) Kim, H.; Farrell, A. C.; Senanayake, P.; Lee, W.-J.; Huffaker, D. L. Monolithically Integrated InGaAs Nanowires on 3D Structured Silicon-on-Insulator as a New Platform for Full Optical Links. *Nano Lett.* **2016**, *16*, 1833–1839.
- (12) Mayer, B.; Janker, L.; Loitsch, B.; Treu, J.; Kostenbader, T.; Lichtmannecker, S.; Reichert, T.; Morkötter, S.; Kaniber, M.; Abstreiter, G.; Gies, C.; Koblmüller, G.; Finley, J. J. Monolithically Integrated High- β Nanowire Lasers on Silicon. *Nano Lett.* **2016**, *16*, 152–156.
- (13) Schuster, F.; Kapraun, J.; Malheiros-Silveira, G. N.; Deshpande, S.; Chang-Hasnain, C. J. Site-Controlled Growth of Monolithic InGaAs/InP Quantum Well Nanopillar Lasers on Silicon. *Nano Lett.* **2017**, *17*, 2697.
- (14) Lu, F.; Bhattacharya, I.; Sun, H.; Tran, T.-T. D.; Ng, K. W.; Malheiros-Silveira, G. N.; Chang-Hasnain, C. Nanopillar Quantum-Well Lasers Directly Grown on Silicon with Silicon-Transparent Waveguides. *Optica* **2017** Submitted for publication.
- (15) Wada, H.; Kamijoh, T. Room-Temperature CW Operation of InGaAsP Lasers on Si Fabricated by Wafer Bonding. *IEEE Photonics Technol. Lett.* **1996**, *8*, 173–175.
- (16) Park, H.; Fang, A. W.; Kodama, S.; Bowers, J. E. Hybrid Silicon Evanescent Laser Fabricated with a Silicon Waveguide and III-V Offset Quantum Wells. *Opt. Express* **2005**, *13*, 9460.
- (17) Wieland, J.; Melchior, H.; Kearley, M. Q.; Morris, C. R.; Moseley, A. M.; Goodwin, M. J.; Goodfellow, R. C. Optical Receiver Array in Silicon Bipolar Technology with Selfaligned, Low Parasitic III/V Detectors for DC-1 Gbit/S Parallel Links. *Electron. Lett.* **1991**, *27*, 2211.
- (18) Chen, R.; Ng, K. W.; Ko, W. S.; Parekh, D.; Lu, F.; Tran, T.-T. D.; Li, K.; Chang-Hasnain, C. Nanophotonic Integrated Circuits from Nanoresonators Grown on Silicon. *Nat. Commun.* **2014**, *5*, n/a.
- (19) Borg, M.; Schmid, H.; Moselund, K. E.; Signorello, G.; Gignac, L.; Bruley, J.; Breslin, C.; Das Kanungo, P.; Werner, P.; Riel, H. Vertical III–V Nanowire Device Integration on Si(100). *Nano Lett.* **2014**, *14*, 1914–1920.
- (20) Ko, W. S.; Bhattacharya, I.; Tran, T.-T. D.; Ng, K. W.; Adair Gerke, S.; Chang-Hasnain, C. Ultrahigh Responsivity-Bandwidth Product in a Compact InP Nanopillar Phototransistor Directly Grown on Silicon. *Sci. Rep.* **2016**, *6*, 33368.
- (21) Deshpande, S.; Bhattacharya, I.; Malheiros-Silveira, G.; Ng, K. W.; Schuster, F.; Mantei, W.; Cook, K.; Chang-Hasnain, C. Ultra-Compact Position-Controlled InP Nanopillar LEDs on Silicon with Bright Electroluminescence at Telecommunication Wavelengths. *ACS Photonics* **2017**, *4*, 695.
- (22) Malheiros-Silveira, G. N.; Wiederhecker, G. S.; Hernández-Figueroa, H. E. Dielectric Resonator Antenna for Applications in Nanophotonics. *Opt. Express* **2013**, *21*, 1234.